PHYSICAL REVIEW B VOLUME 16, NUMBER 1 1 JULY 1977

^{93}Nb nuclear magnetic resonance and relaxation in Nb_3Sn, Nb_3Al, and Nb_3Sb†

F. Y. Fradin and G. Cinader*
Argonne National Laboratory, Argonne, Illinois 60439
(Received 7 February 1977)

The high-temperature superconductors Nb_3Sn and Nb_3Al and the low-temperature superconductor Nb_3Sb have been investigated by ^{93}Nb nuclear magnetic resonance and spin-lattice relaxation-time T_1 measurements. The relaxation-time results combined with electronic-heat-capacity results indicate that Nb_3Sn and Nb_3Al have similar densities of states at the Fermi level in the δ and π subbands, whereas Nb_3Sn has a much larger density of states at E_F in the σ subband. Nb_3Sb is a low density-of-states material. Large enhancements of $(T_1T)^{-1}$ ($\sim$300%) are found for $T \simeq T_c$ in Nb_3Al and Nb_3Sn. The dependence of $(T_1T)^{-1}$ on $(T-T_c)/T_c$ suggests that highly anisotropic pair fluctuations exist well above T_c.

I. INTRODUCTION

The intermetallic compounds of the A-15 phase (Cr_3O-type) have been of considerable interest for a number of years because of their high superconducting transition temperatures T_c and upper critical magnetic fields H_{c2}. In the attempt to understand the influences of the normal state electron and phonon properties on the systematics of T_c or the phonon mediated mass enhancement λ, it has become apparent that important differences exist between the V_3X and Nb_3X compounds, where X is a nontransition element. Most importantly, the systematic increase of T_c with an increase in electron density of states at the Fermi level $N(0)$ found in the V_3X compounds is not found in the Nb_3X compounds. For V_3X compounds, ^{51}V nuclear-magnetic-resonance (NMR) and nuclear spin-lattice relaxation-time T_1 measurements have been quite important in determining the systematics of the subband components of $N(0)$.[1,2] However, because of the much larger value of the nuclear-electric quadrupole interaction for ^{93}Nb in the Nb_3X compounds, no reliable T_1 measurements have been reported for these compounds.[3]

In the present paper, we report our ^{93}Nb NMR results on Nb_3Sn, Nb_3Al, and Nb_3Sb. We have successfully employed a high-rf-power broadband saturation technique to obtain reliable spin-lattice relaxation-time values.

The technique is described in Sec. II. The spectra and relaxation data are presented in Sec. III. In Sec. IV we discuss the results, with emphasis on the information that the T_1 data yields for the subband density of states $N^m(0)$. We find that the two high-T_c compounds Nb_3Sn and Nb_3Al, which have quite different values of $N(0)$, have similar values of certain $N^m(0)$, whereas the low-T_c compound Nb_3Sb has a very low value of all the $N^m(0)$. In addition, we find a large contribution to $1/T_1$, due to quasi-one-dimensional pair fluctuations for $T \gtrsim T_c$ in Nb_3Sn and Nb_3Al. In Sec. V the conclusions are summarized.

II. EXPERIMENTAL PROCEDURE

The fine powder samples used in the NMR study were obtained by crushing ingots in a ball mill and passing the powder through a 400-mesh sieve. The Nb_3Al sample was made by arc melting and had a lattice parameter a_0 of 5.187(1) Å. To avoid precipitation of Nb_2Al, the sample was not heat treated. The Nb_3Sn sample was made by hot pressing to a density of 82% of theoretical. The temperature and pressure were gradually raised to 1200 °C and 8600 psi and maintained there for 11 h. A small concentration of α-Nb and tin was found in addition to the A-15 phase with a_0 = 5.291(1) Å. The Nb_3Sb sample was made with 99.05-at.% enriched ^{123}Sb to suppress the ^{121}Sb resonance that interferes with the ^{93}Nb resonance. The sample was made by an iodide transport technique. The mixture of Sb and Nb powders was sealed in an evacuated quartz capsule with I_2. An initial reaction was carried out at 900 °C for 24 h. The capsule was then placed in a gradient furnace for four days, with the lower end of the capsule at 880 °C and the upper end at 1062 °C. Small single crystals were obtained with $a_0 = 5.262(1)$ Å.

The superconducting transition temperature T_c was measured, using an inductance bridge and a calibrated Ge thermometer, and found to be 18.25 K for Nb_3Al and 17.65 K for Nb_3Sn. No transition was found for $Nb_3{}^{123}Sb$ above 2.13 K. A T_c value of 0.2 K has been reported for a similarly prepared sample of Nb_3Sb.[4] Crushing the ingots increased the transition width ~1–3 deg. The powders were annealed, which resulted in somewhat reduced transition widths. The susceptibilities were measured above T_c, and no indication of paramagnetic impurities was found. The niobium used in all samples was from the same batch, and hence, the same impurity concentra-

tion is expected in all samples (the Nb was nominally 99.8% pure; the Al, Sn, and Sb were of much higher purity).

The ^{93}Nb resonance was measured with a phase-coherent single-coil pulse spectrometer. Line shapes were obtained at a constant frequency of ~44 MHz (supplied by a General Radio frequency synthesizer) by recording the integrated quadrupole echo amplitude as the external magnetic field was swept. The echo signal was obtained by a set of two pulses of roughly 0.5–2 μsec duration with ~80 μsec separation. The exact pulse width was set to obtain a maximum echo amplitude. For the broad spectra of ^{93}Nb in the Nb_3X compounds, the rf level irradiates only a small fraction of the spectral width. The reference phase at the detector was set by symmetrizing the echo signal. Because of the large quadrupole broadening, the signal decay time was usually of the order of 1 μsec. The boxcar integrator gate was centered on the echo, and its width was ~20–30 μsec to ensure a total integration of the echo signal at the sharpest peaks of the NMR spectrum. The effective time constant (learning time) of the boxcar integrator was sufficiently short to follow the signal without distortion at the field sweep rates used. The magnetic field was supplied by a Westinghouse superconducting solenoid. The field of the superconducting solenoid was monitored through the power-supply current I_H. We have calibrated the field by using the signals of the two copper isotopes from the sample rf coil. We assume, during a given field sweep, that $H_{\text{true}} = a + bI_H$, where $|a| \lesssim 100$ G and b is a calibration constant. The sign and magnitude of a depends upon the direction of the field sweep and its rate, because of the presence of the normal state of the persistence switch across the superconducting solenoid (resistor in parallel with an inductor). The values of the gyromagnetic ratios γ_{eff} in metallic Cu used in the calibration are $^{63}\gamma_{\text{eff}} = 1.1312$ kHz/G and $^{65}\gamma_{\text{eff}} = 1.2119$ kHz/G. Values of the ^{93}Nb Knight shift are reported relative to $^{93}\gamma = 1.0407$ kHz/G.

The main experimental difficulty was to obtain accurate values of the spin-lattice relaxation time T_1. In our case, the complete saturation of the nuclear resonances is made difficult by the large quadrupole splittings. Partial saturation leads to a recovery behavior that can be described by a sum of several exponential terms.[5-7] For the case of magnetic hyperfine relaxation processes and $I = \frac{9}{2}$, these are characterized by five time constants for relaxation of the $\frac{1}{2} \rightarrow -\frac{1}{2}$ magnetization (otherwise up to ten time constants are required), i.e., $(\frac{1}{45})T_1$, $(\frac{1}{28})T_1$, $(\frac{1}{15})T_1$, $(\frac{1}{6})T_1$, T_1, and amplitudes that depend on the initial population of the $2I+1$ spin levels. The early time dependence is, in general, dominated by the fastest rate, which is $45T_1^{-1}$ in the present case. Although the recovery of the longitudinal magnetization always tends systematically toward the rate T_1^{-1}, this limiting rate is usually masked by noise or instrument instabilities, unless the fast-relaxation components are strongly suppressed by the initial conditions imposed on the spin system or the signal-to-noise (S/N) ratio is sufficiently high to follow the magnetization recovery for several T_1.

A high S/N ratio was achieved by working in high persistent magnetic fields and high frequencies. Additional improvement was achieved by using a series resonance arrangement in the detection probe, with a half wavelength copper coaxial cable between the sample coil and its tuning capacitor. Maximum induction could be used in this arrangement. Most of the coaxial cable was kept at low temperature, hence reducing losses and yielding a high $Q = \omega L/R_s \simeq 80$ in the detection mode. A Biomation digitizer (0.5 μsec, 8 bits) and a Nicolet signal averager (1024 channel) were used to repetitively accumulate the quadrupole echo signal following recovery of the nuclear magnetization; we obtain $S/N \geq 100$, which enables us to follow the signal recovery to 4–5 T_1.

The main problem was to strongly suppress the high relaxation-rate components. For spectral widths of $\lesssim$1 kG, this can usually be accomplished by using saturating combs composed of a large number of narrow high-intensity rf pulses at the central transition frequency. For effective saturation the comb length is limited by T_1 and the spacing between the pulses is limited by spin diffusion, which is quite long in strongly broadened spectra. Moreover, the number of saturating pulses that can be used is limited by rf heating effects in the sample, which can be quite severe at low temperatures.

Because of the huge quadrupole broadening of our spectra (~10 kG), we could not obtain satisfactory T_1 measurements by applying a conventional saturating comb. In addition to delivering an rf pulse transmitter power of ~20–30 kW to the sample tank circuit (the number of nuclei effected by the rf excitation is, for such broad lines, proportional to the rotating component of the rf field, which was ~200 G), we used a broad rf spectrum that was roughly tailored to the line shape.[8] Using a white noise source and an rf filter of variable Q as the signal source for one of the rf channels of the transmitter, we irradiated a spectrum of ~2–4 MHz full width at half intensity. In this method, we were not limited by spin diffusion and achieved satisfactory saturation [~(80–90)%] for shorter comb lengths. Usually, a comb of ~32–64

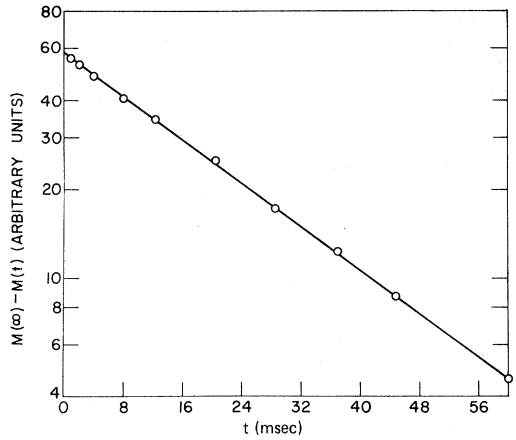

FIG. 1. Recovery of the longitudinal magnetization in Nb_3Sn to its equilibrium value $M(\infty)$ at 19.7 K. Straight line is least-squares fit of the data to Eq. (9), with $T_1 = 26(1)$ msec.

pulses of 2–4 μsec width and 128 μsec separation was sufficient. The rf heating of the sample was found to be negligible using this method, with the sample immersed in a cryogenic liquid of helium, hydrogen, or nitrogen. At a time t after the end of the saturation comb, two rf pulses are transmitted using the second rf channel at the exact phase-detector reference frequency, which was set on the central line to create a quadrupole echo signal that is proportional to that recovered magnetization $M(t)$ of the $\frac{1}{2} \rightarrow -\frac{1}{2}$ transition. The intensity of these detection pulses was weak (≈30 G) so that only the magnetization in the $\frac{1}{2} \rightarrow -\frac{1}{2}$ transition was observed.

An example of a typical recovery curve is shown in Fig. 1 for Nb_3Sn at 19.7 K. The recovery of the signal shows an exponential time dependence for several time constants. The initial saturation is ~90% complete. Results of a similar character were obtained in Nb_3Al, but for Nb_3Sb, multiexponential decays were observed, as shown in Fig. 2.

III. RESULTS

The NMR spectra of ^{93}Nb in Nb_3Al and Nb_3Sn have been measured by Ehrenfreund *et al.*[3] Our results are in good agreement with the published data. In Fig. 3, we show the NMR spectrum of Nb_3Sb at 4.33 K. The peak just below the first high-field satellite is due to ~1% of ^{121}Sb isotope in the sample. This assignment is based upon experiments on a sample of Nb_3Sb made with natural Sb. To analyze the spectra, we must consider the effect of the nuclear-electric quadrupole interaction and the anisotropic Knight shift.

Jones *et al.*[9] have shown that the nuclear Zeeman levels are obtained by adding the expressions for the anisotropic shift (in first order) and the nuclear quadrupole interaction (to second order). We shall assume that the electric-field-gradient (efg) tensor and the magnetic shift tensor are both axially symmetric and the major axes of the two tensors are parallel.

The zeroth order, or pure Zeeman, frequency is the resonance frequency in the metal

$$\nu_0 = \nu_R(1 + K_{\rm iso}). \tag{1}$$

Here, ν_R is the resonance frequency in a diamagnetic reference compound, and $K_{\rm iso} = \frac{1}{3}K_{\parallel} + \frac{2}{3}K_{\perp}$, where $K_{\parallel}$ and $K_{\perp}$ are the Knight shifts parallel and perpendicualr to the major axis of the magnetic shift tensor, respectively.

The satellite frequencies are given in first order by[10]

$$\nu(m \rightarrow m-1) = \nu_0\{1 + (3\mu^2 - 1) \times [a + \tfrac{1}{2}(\nu_Q/\nu_0)(m - \tfrac{1}{2})]\}, \quad m \neq \tfrac{1}{2}. \tag{2}$$

Here, $\mu \equiv \cos\theta$, where θ is the angle between the external magnetic field H_0, and the z axis of the principal axis system and $a \equiv K_{\rm ax}(\nu_R/\nu_0)$, where $K_{\rm ax} = \frac{1}{3}(K_{\parallel} - K_{\perp})$ and $\nu_Q = 3e^2qQ/2I(2I-1)h$. For a random polycrystalline sample, the principal maximum intensity for the satellites occurs when $\mu = 0$, so that resonance peaks appear at

$$\nu(m \rightarrow m-1) = \nu_0\{1 - [a + \tfrac{1}{2}(\nu_Q/\nu_0)(m - \tfrac{1}{2})]\}, \quad m \neq \tfrac{1}{2}. \tag{3}$$

These peaks are shifted in second order by

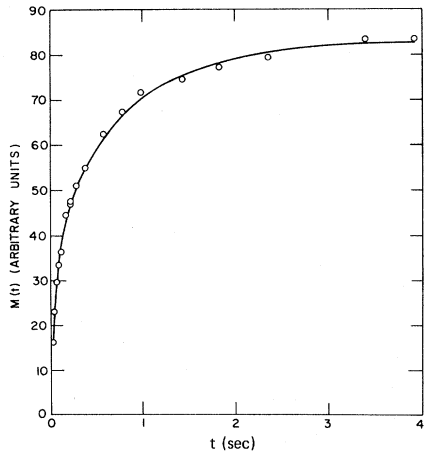

FIG. 2. Recovery of the longitudinal magnetization in Nb_3Sb at 4.3 K. Solid line is the least-squares fit of the data to Eq. (8), yielding $M(t) = 83.1(2)\,[1 - 0.520(4)e^{-t/T_1} - 0.154(6)e^{-6t/T_1} - 0.270(8)e^{-15t/T_1}]$, with $T_1 = 0.806(20)$ sec.

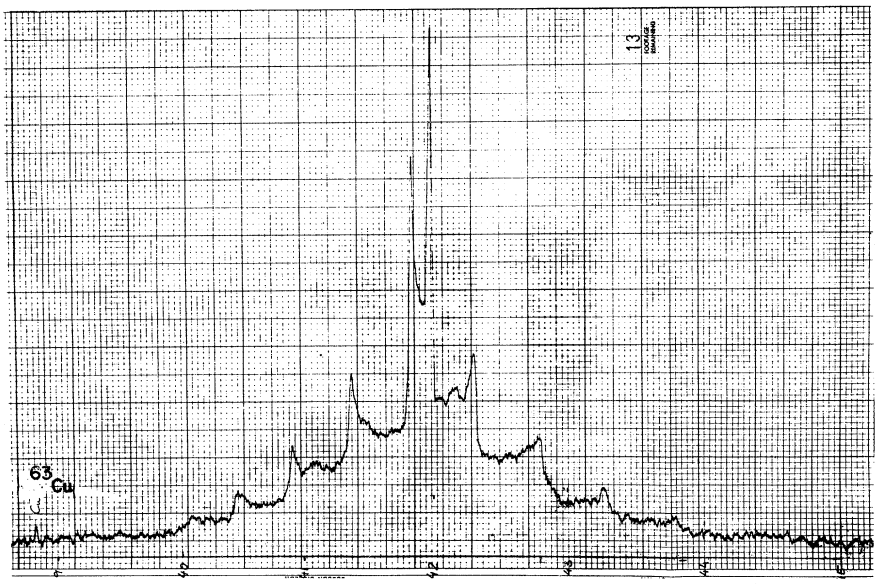

(a)

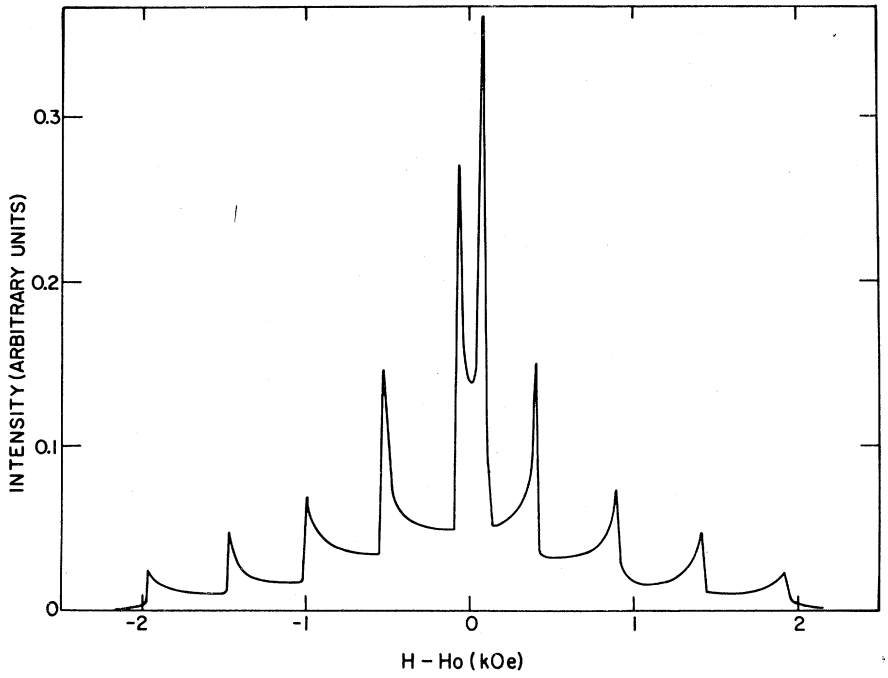

(b)

FIG. 3. (a) Field sweep of the quadrupole echo of Nb_3Sb at 4.33 K and 43.98 MHz. Field increases to the right at 460 Oe per major division. ^{63}Cu resonance in the rf coil is the small peak at the left-hand side of the trace. (b) Synthetic spectra for $e^2Qq/h = 24.2$ MHz and $K_{ax} = -0.08\%$.

$$\Delta\nu(m \rightarrow m-1) = -\tfrac{1}{16}(\nu_Q^2/\nu_0)[3m(m-1) - I(I+1) + \tfrac{3}{2}], \quad m \neq \tfrac{1}{2}. \quad (4)$$

The central transition in a single crystal is given to second order as

$$\nu(\tfrac{1}{2} \leftrightarrow -\tfrac{1}{2}) = \nu_0\{1 + (\nu_Q^2/16\nu_0^2)[I(I+1) - \tfrac{3}{4}] \times (1-\mu^2)(1-9\mu^2) + a(3\mu^2 - 1)\}. \quad (5)$$

To compute a line shape appropriate to a polycrystalline sample, we have, following Cohen and Reif,[11] the shape function

$$P(\nu - \nu_0)d(\nu - \nu_0) = P(\theta)\,d\theta = \tfrac{1}{2}\sin\theta\,d\theta = \tfrac{1}{2}d\mu, \quad (6)$$

$$P(\nu - \nu_0) = \tfrac{1}{2}\left|\frac{d\nu}{d\mu}\right|^{-1}, \quad -1 \leq \mu \leq 1. \quad (7)$$

The synthetic resonance is generated[1,2,12] for each of several values of efg and K_{ax} by folding the intensity distribution function $P(\nu - \nu_0)$, corresponding to Eqs. (2) and (5), with the resonance shape function $g(\nu)$, which is taken as a Gaussian

TABLE I. Knight shift and nuclear electric quadrupole interaction for $^{93}Nb_3X$ compounds.

Compound	K_{ax} (%)	K_{iso} [a] (%)	$\frac{e^2qQ}{h}$ (MHz)	$\lvert eq\rvert$ [b] (10^{14} cgs)	$N_{\gamma_0}(0)$ [c]
Nb_3Sn [d]	>0	+0.70(10)	49	34	1.60
Nb_3Al [d]	+0.15(10)	+0.82(10)	107	74	1.07
Nb_3Sb	−0.08(10)	+0.68(10)	24	17	0.27

[a] ~4 K values.
[b] $^{93}Q = 0.20 \times 10^{-24}$ cm^2.
[c] Reference 4; calculated from McMillan's equation for T_c and the low-temperature heat-capacity data, in units of states/(eV Nb spin).
[d] Ehrenfreund *et al.* (Ref. 3).

function with second moment $\langle \Delta\nu^2 \rangle$. All of these resonance curves are placed on a common frequency scale and summed.

Referring to Fig. 3, we deduced $\nu_Q = 1.005 \pm 0.01$ MHz ($e^2qQ/h = 24.13 \pm 0.25$ MHz) from the satellite splitting, and a best synthetic profile fit to the spectrum was obtained for $K_{ax} = -(0.8 \pm 0.1) \times 10^{-3}$ [Fig. 3(b)]. The center of gravity of each satellite pair, when corrected for the second-order nuclear-electric quadrupole shift of the pair, gives $K_\perp = +7.6 \times 10^{-3}$. Hence, $K_\parallel = 5.2 \times 10^{-3}$ and $K_{iso} = 6.8 \times 10^{-3}$. The values of the nuclear-electric quadrupole interaction and the values of K_{ax} and K_{iso} for the three compounds are listed in Table I.

The ^{93}Nb spin-lattice relaxation data are summarized in Table II for Nb_3Sb, Nb_3Sn, and Nb_3Al. The Nb_3Sb data were fit to a multiexponential time dependence for the recovery of the nuclear magnetization of the $(\frac{1}{2} \rightarrow -\frac{1}{2})$ transition. We found it necessary to retain the three slowest exponential terms. That is, the magnetization was fit to

$$M(t) = M(\infty)(1 - A_1 e^{-t/T_1} - A_2 e^{-6t/T_1} - A_3 e^{-15t/T_1}). \quad (8)$$

For Nb_3Sn, all recovery curves were well described by a single exponential fit:

$$M(t) = M(\infty)[1 - A_1 e^{-t/T_1}]. \quad (9)$$

For Nb_3Al, the recovery was fit to Eq. (8) or Eq. (9). But because the recovery in Nb_3Al was nearly single exponential, the coefficients A_2 and A_3 are quite small compared with A_1. In Table II, t_{max} is the maximum time for which recovery data were obtained. The increase of T_1T with temperature found for Nb_3Sn and Nb_3Al is not observed for Nb_3Sb. Although the isotopically enriched sample of Nb_3Sb is too small to obtain accurate values

TABLE II. Spin-lattice relaxation results for $^{93}Nb_3X$.

Compound	T (K)	T_1 (msec)	Error [a] (%)	t_{max}/T_1 [b]	Fit type [c]	A_1 [d]	T_1T (sec K)
Nb_3Sb	4.3	806	2.5	5	M.E.	0.52	3.46
Nb_3Sn	77.0	21.2	5	4	S.E.	0.95	1.63
	67.0	24.7	5	3	S.E.	0.93	1.66
	19.7	26.0	5	2.5	S.E.	0.90	0.51
	14.15	32.0	5	1.5	S.E.	0.87	0.45
	14.15	30.2	4	4	S.E.	0.95	0.43
Nb_3Al	77.0	20.3	7	5	S.E.	0.80	1.56
	76.0	20.7	6	5.5	S.E.	0.76	1.57
	66.6	21.8	8	5	S.E.	0.88	1.45
	19.5	25.7	6	4	S.E.	0.78	0.50
	19.4	28.0	6	4.5	S.E.	0.80	0.54
	19.07	22.7	3	6	M.E.	0.89	0.43
	18.1	25.7	5	6	S.E.	0.89	0.465
	17.2	24.7	5	6	S.E.	0.90	0.42
	15.95	24.4	2	6	M.E.	0.83	0.39

[a] 90% confidence level, uncertainty in T_1.
[b] t_{max} = maximum time for which data were obtained.
[c] M.E., multiexponential, Eq. (8); S.E., single exponential, Eq. (9).
[d] See Eqs. (8) and (9).

of T_1T at liquid nitrogen temperature, some indication exists that T_1T becomes somewhat smaller at 66 K.

IV. DISCUSSION

Although the strength of the nuclear-electric quadrupole interaction at ^{51}V in the V_3X compounds shows a systematic trend with the density of states at the Fermi level,[1,13] this is clearly not the case for the Nb_3X compounds.[3] In Table I, we have listed the specific-heat value $N_\gamma(0)/(1+\lambda)=N_{\gamma_0}(0)$, corrected for the electron mass renormalization. The lack of correlation of e^2qQ/h with $N_{\gamma_0}(0)$ could be due to the dominance of the point-charge contribution to the electric field gradient q. Based on theoretical calculations of the Sternheimer[14] antishielding factors $(1-\gamma_\infty)$, one can estimate that $1-\gamma_\infty$ should be about four times larger for ^{93}Nb than for ^{51}V. Thus, we would expect the point-charge contribution in the Nb_3X compounds to be more important, relative to the conduction-electron contribution[13] to q, when compared with the V_3X compounds. In addition, $N(0)$ is generally larger for the V_3X compounds when compared with the Nb_3X compounds. This leads to a larger conduction-electron contribution to q in the V_3X compounds.

Although $N(0)$ for Nb_3Sn is ~50% larger than that of Nb_3Al, the values of T_1T at 66–77 K differ by <10%. To understand the relaxation rates, we must consider the various contributions to the hyperfine field at the ^{93}Nb nucleus for the appropriate point symmetry in the Nb_3X compounds.

The A-15 (Cr_3O type) structure in which the Nb_3X compounds crystallize is a cubic lattice with the X atoms on a body-centered-cubic sublattice. We focus attention on the Nb sites that have tetragonal symmetry. The point group is $D_{2d}(\bar{4}2m)$, and the niobium atoms lie on chains arranged in three orthogonal families. In Table III, we list the irreducible representation of the d-wave function ($l=2$) for a niobium atom on a chain with the axis parallel to the $\vec{z}$ direction.

TABLE III. Irreducible representation of $D_{2d}(l=2)$.

Bases	Assignment	Atomic functions	Spherical[a] harmonics
A_1	σ_z	$(5/4\pi)^{1/2}(3z^2-r^2)/2r^2$	Y_2^0
E	π_{1z}	$(15/4\pi)^{1/2}zx/r^2$	Y_2^1,c
E	π_{2z}	$(15/4\pi)^{1/2}zy/r^2$	Y_2^1,s
B_1	δ_{1z}	$(15/16\pi)^{1/2}(x^2-y^2)/r^2$	Y_2^2,c
B_2	δ_{2z}	$(15/4\pi)^{1/2}xy/r^2$	Y_2^2,s

[a] $Y_l^{m,c}\equiv(Y_l^m+Y_l^{-m})\sqrt{2}$; $Y_l^{m,s}=-i(Y_l^m-Y_l^{-m})/\sqrt{2}$; $Y_l^m(\theta,\phi)$ are normalized spherical harmonics. The polar angle θ is measured with respect to a z axis parallel to the tetragonal or chain axis.

The important contributions to the observed relaxation rates in transition metals arise from core-polarization[15] and orbital[16] hyperfine interactions with the d component of the conduction-electron wave function at the Fermi level and from the contact[17] hyperfine interaction with the s component. Conduction-electron contributions associated with magnetic dipole and electric quadrupole[18] hyperfine interactions are usually quite small. (For example, we estimate the electric quadrupole contribution in Nb_3Al is <0.1% of the measured relaxation rate.) Fradin and Zamir[1] discussed the strong dependence of the various contributions to the spin-lattice relaxation rate on the point-group symmetry properties of the d component of the conduction-electron wave function, i.e., the ratio of the A_1, E, B_1, and B_2 orbital admixtures, in tetragonal symmetry.

In the absence of s-d mixing, spin-orbit coupling, and Coulomb enhancement effects, the spin-lattice relaxation rate $R=(T_1T)^{-1}$ in tight binding can be expressed as[1]

$$R=\frac{4\pi}{\hbar}(\gamma_n\hbar)^2k_B[N(0)^2]\sum_i P_i^2(K_i^{(1)}+K_i^{(2)}\sin^2\theta), \tag{10}$$

where γ_n is the nuclear gyromagnetic ratio, k_B is the Boltzmann constant, and $N(0)$ is the bare density of states at the Fermi level for one direction of spin. The sum is over the three hyperfine interactions: s-contact $P_s=\rho H_{\rm hfs}^s$, d-spin core-polarization $P_d=(1-\rho)H_{\rm hfs}^d$, and d-orbital $P_{\rm orb}=(1-\rho)H_{\rm hfs}^{\rm orb}$. Here, ρ is the average fractional s character at the Fermi level $\rho=N_s(0)/N(0)$, θ is the angle between the tetragonal axis and the applied field, and $K_i^{(1)}$ and $K_i^{(2)}$ are functions[1] of the orbital admixture coefficients $F^{\Gamma(m)}$. The $F^{\Gamma(m)}$ terms are the average values of the fractional admixture coefficients at the Fermi level that have the same value for all m, which form a basis for a given irreducible representation $\Gamma(m)$,

$$F^{\Gamma(m)}=\sum_\mu\sum_k |C_{\mu mk}|^2[\delta(E_{\mu k}-E_F)][N(0)N]^{-1}, \tag{11}$$

where the $C_{\mu k}$ terms are the fractional admixture coefficients, $E_{\mu k}$ is the energy of the electron with band index μ and wave vector k, E_F is the Fermi energy, and $N(0)N$ is the total number of states per unit energy interval at the Fermi level for one direction of spin.

If the A_1 functions are expressed as linear combinations of the form $\xi_{\mu\vec{k}}Y_0^0+(1-\xi_{\mu\vec{k}}^2)^{1/2}Y_2^0$, the s-d interference term is given by[1]

$$R_{s-d} = (8\pi/\hbar)(\gamma_n\hbar)^2[N(0)]^2 H_{\rm hfs}^{(s)} H_{\rm hfs}^{(d)} \times \langle\langle (F_{\mu\vec{k}}^{A_1})^2 \xi_{\mu\vec{k}}^2 (1 - \xi_{\mu\vec{k}}^2)\rangle\rangle , \quad (12)$$

where the angular brackets denote an average over the Fermi surface. Since $H_{\rm hfs}^{(s)}$ and $H_{\rm hfs}^{(d)}$ are of opposite sign, this term interferes destructively with Eq. (10).

The foregoing analysis contains two tacit assumptions. First, it was assumed that the expansion of the conduction-electron wave functions at the Fermi level could be limited to $l=0$ and $l=2$ atomic functions, i.e., $N(0)=N_s(0)+N_d(0)$. It is likely, however, that the $l=1$ admixture is often comparable to the $l=0$ admixture. Nevertheless, the $l=1$ hyperfine interaction may be safely neglected, since p hyperfine fields are generally quite small compared with s and d hyperfine fields. The major effect of an appreciable admixture at the Fermi level is the reduction of $N(0)$ relative to the total bare-electron density of states by an amount proportional to the fractional p character. This reduction is probably small since the density of states in transition metals is dominated by the d-band contributions. Second, a potentially more serious defect in the analysis is the assumption that the four d orbitals have identical radial dependences. In other words, the d-spin and d-orbital hyperfine fields are assumed to be constants. This assumption is reasonable only if the potential within the atomic volume is nearly spherically symmetric.

We have consciously ignored the effects of electron-electron exchange enhancement on T_1, because these effects should be small in high T_c superconductors. As is well known, phonon renormalization effects do not enter the relaxation rate.[19]

We first focus attention on the values of T_1 for $T \gg T_c$. For the hyperfine fields on Nb, we use the earlier estimates[3,20] $H_{\rm hfs}^{s}(5s) = 2.48\times10^6$Oe/$\mu_B$, $H_{\rm hfs}^{d}(4d\text{-spin}) = -0.21\times10^6$Oe/$\mu_B$, and $H_{\rm hfs}^{\rm orb}(4d\text{-orb}) = 0.28\times10^6$Oe/$\mu_B$. Furthermore, we restrict the total density of states at the Fermi level to that derived from the low-temperature heat capacity and McMillans equation for T_c (i.e., the values of $N_{\gamma_0}(0)$ listed in Table I). Then Eqs. (10) and (12) for the spin-lattice relaxation rate are given in terms of four free parameters, i.e., three independent orbital admixture coefficients and the s fraction at the Fermi level. Here, we assume that $\langle\xi^2(1-\xi^2)\rangle$ can be replaced in Eq. (12) by $\rho(1-\rho)/(F^\sigma)^2$. Furthermore since F^{δ_1} and F^{δ_2} enter the relaxation rate in the identical manner, we will take $F^\delta = F^{\delta_1} + F^{\delta_2}$, with either F^{δ_1} or $F^{\delta_2} = 0$. Extension to other choices of $F^{\delta_1}/F^{\delta_2}$ is easily made. Thus, we are left with three free parameters for the relaxation rate. In Fig. 4, the solutions are plotted as $N^\sigma(0)$ versus $N^\delta(0)$ for various values of $N_s(0)$. We note that the range of solutions for each of the three compounds is quite close to the straight lines of the loci of $N^\pi(0)=0$. The solutions fall in fairly small regions of $N^\sigma(0), N^\delta(0)$ space for reasonable values of $N_s(0)$ between 0 and 0.12 states/(eV Nb spin). In fact, we have checked the solutions with the value of $H_{\rm hf}^{d}(4d\text{-spin})$ halved and find qualitatively similar results. This insensitivity is primarily due to the cancellation effect of the s-d cross terms in the relaxation rate.

Although the solutions for the relaxation rates of the three compounds, shown in Fig. 4, indicate small values of $N^\pi(0)$ and values of $N_s(0) \cong 0.06 \pm 0.06$ (eV Nb spin)$^{-1}$, a large variability in the ratio of $N^\sigma(0)/N^\delta(0)$ occurs. The band-structure calculations[21,22] on the Nb_3X compounds have large uncertainites, relative to the scale in energy of the sharp structural features, in the positions of the various bands. However, the calculations indicate that the density of states in the σ subband is small. Typical solutions that represent minimum values of $N^\sigma(0)$ for a given value of $N_s(0)$ are listed in Table IV. Although the absolute values of the subband densities of states at the Fermi level given in Table IV have a reliability of about ±30%, the

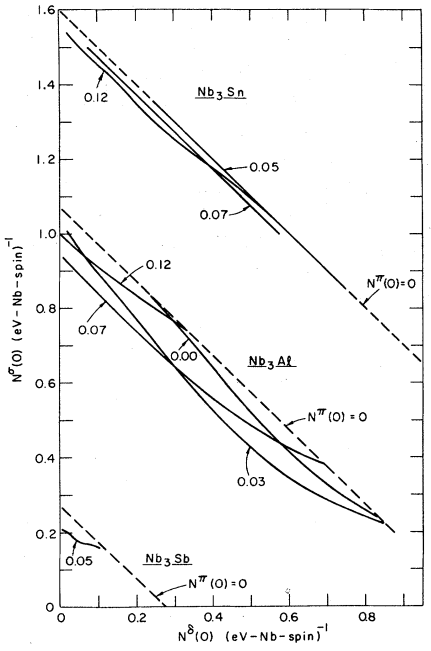

FIG. 4. Plot of loci of subband density of states that are solutions of Eqs. (10) and (12) for indicated values of $N_s(0)$. The values of $R=(T_1T)^{-1}$ of 0.285, 0.637, and 0.625 (sec. K)$^{-1}$ and the values of $N(0)$ of 0.27, 1.07, and 1.60 (eV Nb spin)$^{-1}$ are used for Nb_3Sb, Nb_3Al, and Nb_3Sn, respectively.

TABLE IV. Relaxation rates and subband density of states.

[States/(eV Nb spin)]	Nb_3Sb	Nb_3Al	Nb_3Sn
$N^{\sigma}(0)$	0.16	0.40	0.86
$N^{\delta}(0)$ [a]	0.10	0.65	0.74
$N^{\pi}(0)$	0.01	0.02	0.00
$N(0)$ [b]	0.27	1.07	1.60
$\rho = N_s(0)/N(0)$	0.185	0.047	0.044
$(\sec K)^{-1}$			
R_s	0.397	0.397	0.778
R_d	0.025	0.620	1.33
R_{orb}	0.010	0.074	0.00
R_{s-d}	−0.148	−0.470	−1.49
R_{tot}	0.284	0.621	0.625
R_{exp}	0.285	0.637	0.625

[a] $N^{\delta}(0)=N^{\delta 1}(0)+N^{\delta 2}(0)$ with either $N^{\delta 1}(0)$ or $N^{\delta 2}(0)=0$.
[b] Heat-capacity values corrected for mass enhancement (Ref. 4).

relative values are probably reliable to better than ±10%. We see the major difference in the total density of states for Nb_3Sn, compared with Nb_3Al, is that Nb_3Sn has a much larger value of $N^{\sigma}(0)$, whereas $N^{\delta}(0)$ is similar for the two compounds. The Fermi level in Nb_3Sb apparently falls in a valley in the δ subbands.

The well-known correlation of λ (or T_c) with $N(0)$ in the V_3X compounds[4] is shown in Fig. 5. The correlation is principally due to the fact that $N(0)$ is dominated by $N^{\pi}(0)+N^{\delta}(0)$. Likewise (referring to Fig. 5), if we ignore $N^{\sigma}(0)$, a similar correlation is found for the Nb_3X compounds. We note that the $l=2$ wave functions of σ symmetry (Table III) are expected to have the largest intrachain overlap. It would be interesting to see if the various contributions to λ could be understood in terms of the different magnitudes of the two-center overlap integrals[23] (intrachain and interchain) that characterize the d states of σ symmetry from π and δ symmetries.

Large enhancements of $R \equiv (T_1T)^{-1}$ can be seen (Fig. 6) for temperatures T such that $|T-T_c|/T_c \lesssim 0.2$ in Nb_3Al. For temperatures well below T_c, T_1 becomes exponentially long. The enhancement $\Delta R \cong R - R_{LN_2}$, where R_{LN_2} is the value at liquid-nitrogen temperatures, approaches 300% of R_{LN_2} for both Nb_3Al and Nb_3Sn. These enhancements can be compared with the roughly 30% enhancement[3] of R for ^{27}Al in Nb_3Al. (The magnitude of the enhancements in high T_c V_3X compounds is not clear.[24]) If the large enhancement is due to fluctuations in the gap parameter,[25] the magnitude for ^{93}Nb could be associated with the large degree of anisotropy of the d states at the Fermi level.[26] Only a fraction of this anisotropy of the d states will be important for the ^{27}Al relaxation because of s-d hybridization.

Maniv and Alexander have shown, for a pure three-dimensional system, that the relaxation rate enhancement ΔR due to pair fluctuations is given by

$$\Delta R/R_0 \sim B \ln[(T-T_c)/T_c + A/T^2]^{-1}. \quad (13)$$

They estimate that for Nb, $B=\pi^2/(2k_F\xi_0)^2 \lesssim 10^{-3}$, where k_F is the Fermi wave vector and ξ_0 is the coherence length. In Eq. (13), R_0 is the value of $(T_1T)^{-1}$ in the absence of fluctuations. Obviously, the observed enhancements in Nb_3Al and Nb_3Sn are much larger than predicted by Eq. (13).

Recently, Maniv[28] has calculated ΔR for an assumed quasi-one-dimensional subband for the superconducting electrons. In the clean limit where the mean-free path $l \gg \xi_0$, he finds

$$\Delta R/R_0 \sim \tfrac{1}{8}\pi\{\ln[t+(\xi_0/l)^2+X^2]-\ln[t+(\xi_0/l)^2]\}X^{-2} - (8/\pi)\{(t+X^2)^{1/2}-t^{1/2}\}X^{-2}, \quad (14)$$

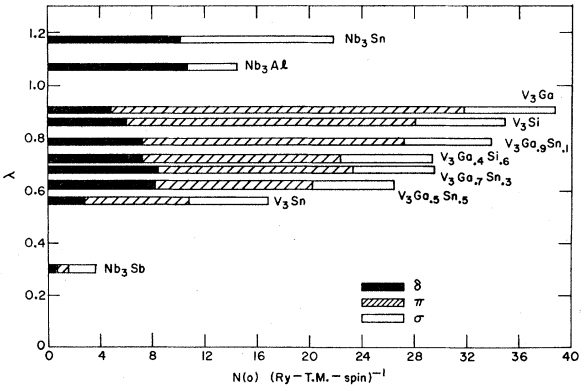

FIG. 5. Dependence of the strength of the electron-phonon interaction on the bare subband density of states for the A-15 compounds.

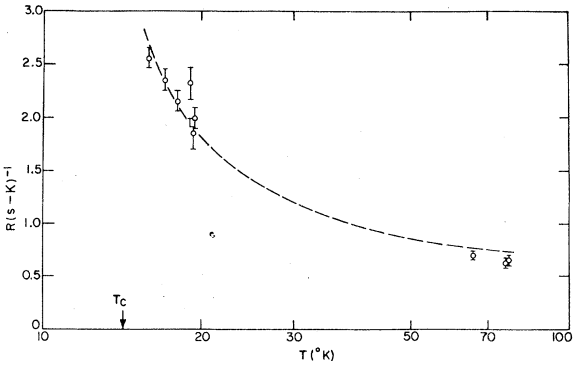

FIG. 6. Temperature dependence of $R=(T_1T)^{-1}$ for Nb_3Al. The curve is a least-squares fit of the data above T_c to Eq. (14).

where $t=\ln(T/T_c)$, $X=X_0(T_c^0/T)$, $\xi_0=v_F/(\sqrt{2}\pi T)$, $X^0=2c^2/(k_Fa)^2(E_F/T_c^0)$, T_c^0 is the mean-field temperature of the phase transition, v_F is the Fermi velocity, c^2 is the effective-mass anisotropy, a is the lattice spacing, and E_F is Fermi energy. In Fig. 6 we have fit the relaxation data of Nb_3Al to Eq. (14), where we have assumed that R_0 is dominated by the d-spin core-polarization term, in agreement with the estimates for Nb_3Al in Table IV. The nonlinear least-squares fit with standard deviation $\sigma=0.10$ (s K) is obtained for the following parameters: $T_c=14.2(7)$ K, $R_0=0.59(10)$ (sec K)$^{-1}$, $X_0T_c^0=12.4(12)$ K, and $T\xi_0/l\lesssim 0.1$ K. The coefficients obtained for the first and second terms in Eq. (14) are $1.01(19)/R_0$ and $0.96(40)/R_0$, respectively. Although the parameters are not very well defined, it is clear that the large value of $X_0T_c^0$ implies a very large effective-mass anisotropy, i.e., $c^2M_{zz}/M_{xx}=3.7\times10^{-3}$. Although this anisotropy is inconsistent with published band-structure calculations,[21] the calculations are too primitive to give reliable mass anisotropies.

Finally, we note that susceptibility measurements on Nb_3Al indicate no significant temperature dependence nor any significant paramagnetic impurity. Additional investigations of the magnetic field dependence of R for $T\lesssim 1.25T_c$ are needed to fully describe the pair-fluctuation effects on T_1.

V. CONCLUSIONS

The ^{93}Nb nuclear spin-lattice relaxation rates in Nb_3Sb, Nb_3Al, and Nb_3Sn are dominated by the Fermi contact and core-polarization contributions. The lack of significant orbital contribution is due to the quite small density of states at E_F in the π subband $N^\pi(0)$. The larger total density of states at the Fermi level in Nb_3Sn relative to Nb_3Al is due to the difference in $N^\sigma(0)$, which appears to have little effect on the strength of the electron-phonon interaction. Large enhancements of $(T_1T)^{-1}$ are found in Nb_3Al and Nb_3Sn for $T\lesssim 1.25T_c$. The functional dependence of $(T_1T)^{-1}$ on temperature suggests that highly anisotropic pair fluctuations exist well above T_c. The anisotropy could be due to the strong δ component of the wave functions at the Fermi level.

ACKNOWLEDGMENTS

The authors express their appreciation to J. W. Downey for his assistance in the preparation of the Nb_3X compounds. The authors acknowledge Dr. T. Maniv for helpful discussions of his theoretical work on pair fluctuation enhancements prior to publication.

[1]F. Y. Fradin and D. Zamir, Phys. Rev. B 7, 4861 (1973).
[2]F. Y. Fradin and J. D. Williamson, Phys. Rev. B 16, 2803 (1974).
[3]E. Ehrenfreund, A. C. Gossard, and J. H. Wernick, Phys. Rev. B 4, 2906 (1971).
[4](a) G. S. Knapp, S. D. Badar, and Z. Fisk, Phys. Rev. B 13, 3783 (1976); (b) F. Y. Fradin, G. S. Knapp, S. D. Bader, G. Cinader, and C. W. Kimball, in *Proceedings of the Second Rochester Conference on Superconductivity in d- and f-band Metals*, edited by D. H. Douglass (Plenum, New York, 1976), p. 297.
[5]E. R. Andrew and D. P. Tunstall, Proc. Phys. Soc. Lond. 78, 1 (1961).
[6]W. W. Simmons, W. J. O'Sullivan, and W. A. Robinson, Phys. Rev. 127, 1168 (1962).
[7]A. Narath, Phys. Rev. 162, 320 (1967).
[8]G. Cinader and F. Y. Fradin (unpublished).
[9]W. H. Jones, Jr., T. P. Graham, and R. G. Barnes, Phys. Rev. 132, 1898 (1964).
[10]B. R. McCart and R. G. Barnes, J. Chem. Phys. 48, 127 (1968).
[11]M. H.Cohen and F. Reif, in *Solid State Physics*, edited by F. Seitz and D. Turnbull (Academic, New York, 1957).
[12]A. J. Arko, F. Y. Fradin, and M. B. Brodsky, Phys. Rev. B 8, 4104 (1973).
[13]R. E. Watson, A. C. Gossard, and Y. Yafet, Phys. Rev. 140, A375 (1965).
[14]R.L. Sternheimer, Phys. Rev. 159, 266 (1967); and private communication.
[15]Y. Yafet and V. Jaccarino, Phys. Rev. 133, A1630 (1964).
[16]Y. Obata, J. Phys. Soc. Jpn. 18, 1020 (1963).
[17]J. Korringa, Physica (Utr.) 16, 601 (1950).
[18]A. H. Mitchell, J. Chem. Phys. 26, 1714 (1957).
[19]L. P. Kadanoff, Phys. Rev. 132, 2073 (1963).
[20]W. Low, J. Phys. Soc. Jpn. 39, 1246 (1968).
[21]L. F. Mattheiss, Phys. Rev. B 12, 2161 (1975).
[22]G. Barak, I. B. Goldberg, and M. Weger, J. Phys. Chem. Solids 36, 847 (1975).
[23]C. M. Varma and R. C. Dynes, in Ref. 4(b), p. 507.
[24]B. G. Silbernagel, M. Weger, W. G. Clark, and J. H. Wernick, Phys. Rev. 153, 535 (1967); B. G. Silbernagel and J. H. Wernick, Phys. Rev. B 5, 3355 (1972).
[25]T. Maniv and S. Alexander, Solid State Commun. 18, 1197 (1976).
[26]M. Weger, T. Maniv, A. Ron, and K. H. Bennemann, Phys. Rev. Lett. 29, 584 (1972).
[27]T. Maniv and M. Weger, J. Phys. Chem. Solids 36, 367 (1975).
[28]T. Maniv (private communication).